Engineering 3 (2017) 596–607

Contents lists available at ScienceDirect

Engineering

journal homepage: www.elsevier.com/locate/eng

Research
Intelligent Manufacturing—Review

# Simulating Resin Infusion through Textile Reinforcement Materials for the Manufacture of Complex Composite Structures

Robert S. Pierce [a,b], Brian G. Falzon [b,*]

[a] Northern Ireland Advanced Composites and Engineering Centre, Belfast BT3 9DZ, UK
[b] School of Mechanical and Aerospace Engineering, Queen's University Belfast, Belfast BT9 5AH, UK

ARTICLE INFO

*Article history:*
Received 28 February 2017
Revised 7 May 2017
Accepted 8 May 2017
Available online 25 September 2017

*Keywords:*
Composite materials
Textile reinforcement
Draping
Infusion
Numerical modeling

ABSTRACT

Increasing demand for weight reduction and greater fuel efficiency continues to spur the use of composite materials in commercial aircraft structures. Subsequently, as composite aerostructures become larger and more complex, traditional autoclave manufacturing methods are becoming prohibitively expensive. This has prompted renewed interest in out-of-autoclave processing techniques in which resins are introduced into a reinforcing preform. However, the success of these resin infusion methods is highly dependent upon operator skill and experience, particularly in the development of new manufacturing strategies for complex parts. Process modeling, as a predictive computational tool, aims to address the issues of reliability and waste that result from traditional trial-and-error approaches. Basic modeling attempts, many of which are still used in industry, generally focus on simulating fluid flow through an isotropic porous reinforcement material. However, recent efforts are beginning to account for the multiscale and multidisciplinary complexity of woven materials, in simulations that can provide greater fidelity. In particular, new multi-physics process models are able to better predict the infusion behavior through textiles by considering the effect of fabric deformation on permeability and porosity properties within the reinforcing material. In addition to reviewing previous research related to process modeling and the current state of the art, this paper highlights the recent validation of a multi-physics process model against the experimental infusion of a complex double dome component. By accounting for deformation-dependent flow behavior, the multi-physics process model was able to predict realistic flow behavior, demonstrating considerable improvement over basic isotropic permeability models.



## 1. Introduction

The commercial aerospace industry is continually striving toward developing stronger and lighter structures. Composite materials, and specifically carbon fiber-reinforced plastics (CFRPs), have become a popular alternative to traditional aluminum alloys. CFRPs offer superior specific strength and stiffness, good structural damping and energy absorption characteristics, and improved fatigue and corrosion resistance [1]. Furthermore, they allow greater flexibility in the design of highly integrated composite structures, which can greatly reduce part count and the need for mechanical fastening. For example, when Airbus introduced a composite vertical tail fin into their A300 and A310 aircraft in 1985, they were able to achieve a 95% reduction in part count from the original metallic design of 2076 parts [2,3]. This resulted in a 95-component structure that was 400 kg lighter, as well as being less expensive to manufacture and assemble [3].

At first, fiber-reinforced composites were only used in the tertiary structures of commercial aircraft, and contributed to a small fraction of the overall structural weight. However, by the mid-1990s, composites had spread to virtually all secondary structures and made up 15%–20% of the total structural composition. At present,

* Corresponding author.
*E-mail address:* b.falzon@qub.ac.uk

http://dx.doi.org/10.1016/J.ENG.2017.04.006

the latest generation of wide-body aircraft, such as the Boeing 787 and Airbus A350, are able to use fiber-reinforced composites for most of the airframe, and composites account for over 50% of the aircraft structural weight [4]. Similar advances are being made in narrow-body aircraft, with the Bombardier C Series and the United Aircraft Corporation Irkut MC-21 achieving composite compositions of over 40% [5]. Fig. 1 shows the increased use of composite materials for commercial aircraft structures since the 1970s.

### 1.1. Materials and manufacturing

Aerospace composites are often manufactured from stacked sheets of unidirectional (UD) carbon fibers that have been pre-impregnated with resin (called "prepregs") and that can produce incredibly stiff and strong laminates. However, to manufacture tougher and more resilient structures, textile reinforcement materials can be used. These are made from woven carbon fiber tows, and can be used in either dry or pre-impregnated formats. Improved handling characteristics, impact resistance, damage tolerance, and notch sensitivity can all be gained at the cost of reduced stiffness (10%–30%) and axial strength (15%–35%), compared with UD prepregs [6]. Furthermore, textile-reinforced composites offer superior out-of-plane mechanical properties, with greater peel strength and reduced crack growth. Dry fabrics also exhibit better forming capabilities over complex tooling, particularly for double curvature geometries, where UD prepregs and tapes often split [6]. The architecture of the textile reinforcement materials also has a considerable effect on the behavior of the composite, meaning that it is possible to tailor the material for a specific role [7]. Hence, a wide variety of woven, knitted, and non-crimp fabrics are used in industry.

The processing of prepreg materials generally relies on a cure cycle under considerable heat and pressure, within an autoclave, to produce a high-quality final part. However, in many cases, an autoclave that is large enough for composite aerostructures can be prohibitively expensive, particularly as autoclaves can cost as much as 3–10 times more than a similarly sized oven [5]. As a result, out-of-autoclave techniques, such as resin infusion under flexible tooling (RIFT) [8], are becoming a popular alternative to the classic prepreg methodology for medium- to large-scale applications at lower production volumes. RIFT methods commonly involve the forming of dry fibrous reinforcement material using a flexible tooling over a rigid mold under vacuum, before resin is allowed to infiltrate through the preform. Once filled, the part is left to cure either under ambient conditions or at elevated temperature inside an oven, while the vacuum is maintained. Such methods can greatly reduce the capital and ongoing costs of manufacturing large composite structures, since an autoclave is not required. By combining out-of-autoclave techniques with the use of dry textile reinforcement materials, material waste can be reduced and shelf life can be increased considerably, compared with perishable prepreg materials [1].

However, reliability and repeatability issues still pose significant concerns for the widespread adoption of resin infusion manufacturing processes in the aerospace industry. These methods rely heavily on the skill and experience of operators through empirical practices, which can result in considerable time and material costs. The weakness of trial-and-error methods is exacerbated by the development of large and highly integrated composite aerostructures. Modern efforts to simulate the resin infusion manufacturing process aim to address the reliability and repeatability concerns in a cost-effective manner.

### 1.2. Process modeling

The resin infusion process is particularly complex to model. Each application fundamentally depends on the mechanical behavior of the reinforcement material as it is being formed, the rheological behavior of the resin during infusion, and even the chemical behavior of the resin system during curing.

Furthermore, these behaviors can change radically at different scales within textile reinforcement materials. The behavior of these materials is typically studied at three hierarchical scales: the macroscale, mesoscale, and microscale. The macroscale refers to the behavior of a whole fabric ply or the entire preform. The mesoscale pertains to the internal architecture of the textile weave, and to the yarns themselves. The microscale focuses on the individual fibers within each yarn. Fig. 2 shows the three different hierarchical scales for textile reinforcement materials.

From a modeling perspective, the macroscale is most commonly adopted as the quickest and simplest approach, assuming homogeneity throughout the textile preform [9]. Mesoscale simulations typically attempt to recreate complex yarn geometries and their interactions within the fabric weave. Hence, mesoscale modeling requires greater computational effort and is not as efficient for simulating large domains. Lastly, microscale modeling usually aims to replicate the distribution and interaction of individual fibers within the yarns. As a result, microscale modeling is the most ambitious approach, and is generally limited to very small domains.

Increases in computational power and in the proliferation of user-friendly software packages have facilitated considerable study into the different aspects of resin infusion at various scales. In general, the manufacturing process is divided into two main fields of research: the physical forming of the reinforcement material, called "draping," and the flow of resin through the reinforcement material, termed "infusion." These two fields are often investigated under the assumption that they are independent processes. However, there is a known link between textile deformation and infusion behavior [10], which is particularly important for complex structures with complex curvature. In light of this link, efforts have been made to develop an "integrated design tool" that predicts the forming,

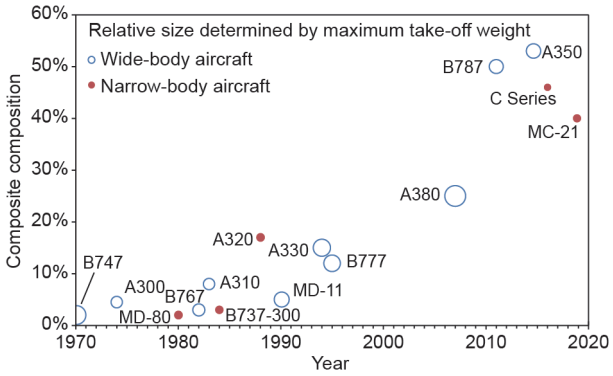


**Fig. 1.** Composite composition of commercial aircraft by structural weight since 1970.

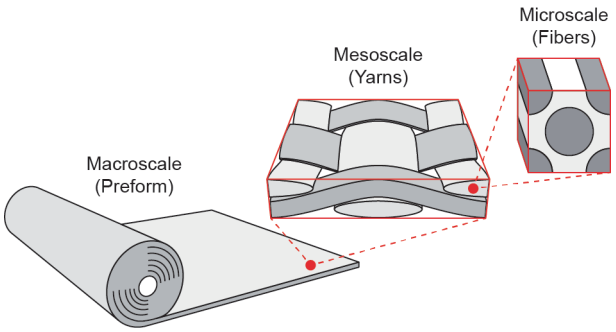


**Fig. 2.** Hierarchical scales for textile reinforcement materials.

infusion, and ultimate performance of a textile-reinforced composite structure [11,12].

This paper reviews the development of process modeling for the infusion of textile-reinforced composite materials, and covers a range of contributing research from the fields of drape modeling, material characterization, and infusion modeling. Recent work by these authors, which demonstrates the use of an advanced multi-physics process model, is also highlighted in this article.

## 2. Drape modeling

The physical response and simulation of textile draping over a complex tooling has been studied for a diverse range of applications. In addition to engineering interests for composite reinforcement materials, the apparel and animation industries have investigated the simulation of fabric draping. The first analytical models for predicting textile-draping behavior employed geometric mapping-based schemes. Next, aesthetic particle-based approaches began appearing in the 1990s for non-engineering applications. However, the most accurate and reliable computational methods now rely on continuum, discrete, or semi-discrete methods. These all require some knowledge of the fabric's mechanical properties in order to simulate deformation behavior realistically. Hence, considerable work has been focused on better understanding and characterizing the mechanisms for fabric deformation in order to support the predictive models.

### 2.1. Mechanical properties

Each modeling approach is founded on different assumptions and may require different mechanical material properties in order to simulate the fabric behavior. For example, in a microscale model that considers small groups of individual fibers, only the elastic properties of the fibers and their interactions may be necessary. Alternatively, in mesoscale simulations of the woven yarns, the properties that are required may be friction and the yarn properties. Macroscale models, on the other hand, often ignore the detail of the yarns and fibers and treat the fabric as a homogenous layer of material. Hence, the mechanical properties of the fabric are required in macroscale simulations; of such properties, in-plane shear is generally considered to be the dominant deformation mechanism [13]. The high tensile stiffness of the reinforcing fibers makes the tensile properties quite important to macroscale fabric behavior. Alternatively, the relatively low bending stiffness of these fabrics is only defined to improve the prediction of wrinkling behavior [14], or is neglected entirely [15].

Since most research aims to understand the macroscale behavior of textile reinforcements for the manufacture of composite structures, the characterization of fabric tensile, shear, and bending properties remains a priority. These properties are typically characterized experimentally, despite a lack of several appropriate standards. However, the use of detailed mesoscale or microscale models in combination with experimentally characterized yarn or fiber properties has also been investigated in order to predict macroscale fabric behavior [16,17]. These predictive methods may be preferable for developing new textiles or for characterizing a range of different weaves made from the same yarns or fibers. Macroscale experimental characterization is usually preferable for determining the properties of a specific pre-existing material.

From a mechanics perspective, draping behavior has proven to be difficult to replicate accurately. Woven warp and weft yarns exhibit considerable tensile strength and stiffness but are highly susceptible to reorientation under shear and bending modes. Therefore, any attempt to model draping must accurately account for the yarn reorientation that results from shear loading [18]. Due to the significance of yarn reorientation, draping studies typically adopt a "shear angle," or $\gamma$ parameter, in order to monitor local deformation. This is a measure of the angular change between the warp and weft yarns in the fabric as a result of deformation, as shown in Fig. 3. In the initial, undeformed state, the warp and weft yarns are perpendicular, corresponding to a shear angle of 0°. However, as shear loading is applied, a trellising behavior occurs and the shear angle increases. Eventually, the gaps between the yarns close and lateral compaction begins, resulting in a "locking" effect and considerable shear resistance. This commonly occurs at shear angles between 30° and 60°, depending on the architecture of the preform. Past this point, further shear loading can result in out-of-plane buckling behavior, also known as wrinkling. For simulation purposes, wrinkling behavior is often neglected, since it is very difficult to replicate. Similarly, draping models typically neglect the slippage of yarns at cross-overs.

#### 2.1.1. Tensile characterization

The tensile properties of the fabric are driven by the stiffness of the fibers within each yarn, but tend to perform only a secondary role during draping. Tensile loading of one yarn direction has been shown to have some influence on the tensile behavior of the other yarn direction, suggesting the need for biaxial characterization in support of draping models [16]. However, biaxial rigs that test cruciform-shaped samples in both the warp and weft yarn directions at various loading rates are challenging to build and operate. As a result, there is no biaxial test standard, and uniaxial "grab" and "strip" [19] tests are often employed instead, under the common assumption that the biaxial behavior is negligible.

#### 2.1.2. Shear characterization

The shear behavior of textile reinforcement materials tends to be highly non-linear. After overcoming initial friction at low loading, fabric yarns are relatively free to rotate under shear loading; however, the shear resistance increases exponentially as the material ultimately reaches a "locked" state. Early investigations of fabric shear behavior employed the Kawabata simple shear test, in which one end of a sample is fixed and the other is sheared transversely [20]. However, this approach was developed for the apparel industry and was found to be limited to small shear deformation for textile

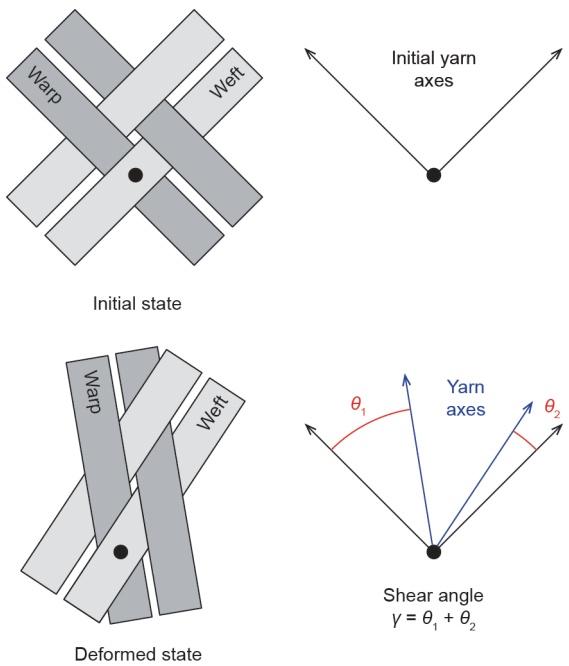


**Fig. 3.** Fabric shearing as a result of deformation and the shear angle definition.

reinforcement materials [21]. Because of this limitation, it is now more popular to use either the picture frame test or the bias extension test, both of which rely on axial testing.

The picture frame test uses square or cruciform-shaped samples that are clamped into a diamond-shaped frame with pin-jointed corners [22]. A standard tensile test machine can then be used to shear the fabric by extending two opposing corners of the frame. This approach shows good repeatability and homogenous deformation throughout the sample; however, clamping and alignment issues are known to influence the results [23]. Alternatively, the bias extension test can be conducted with simple fixtures to avoid any clamping or alignment issues. Rectangular specimens are cut such that the long loading direction bisects the warp and weft yarn directions (the fabric "bias" direction). When tested on a standard tensile testing rig, a heterogeneous distribution of shear deformation results across the sample, where only a central diamond-shaped region undergoes pure shearing. Furthermore, yarn slippage can occur near the clamped edges at higher loads, so optical strain measurement techniques such as digital image correlation (DIC) should be used instead of direct kinematic calculations in order to obtain accurate results [23]. Recent work has demonstrated the coupling of tensile and shear properties with a biaxial bias extension test, in which a transverse load can also be applied to the sample. This work found that additional yarn tension would influence the shear behavior and could also mitigate the onset of out-of-plane buckling (wrinkling) [24]. Ultimately, however, despite significant efforts to establish testing benchmarks [25], there is still no standard for fabric shear testing.

#### 2.1.3. Bending characterization

Textile reinforcement materials exhibit bending hysteresis during loading and unloading as a result of the internal friction among yarns and fibers [26,27]. Therefore, traditional cantilever bending tests, which assume linear elastic bending behavior, are not ideal for these relatively thick and stiff materials. The same is true for the Kawabata Evaluation System bending test for fabrics. Hence, the original cantilever test has been modified by combining mechanical and optical measurement techniques, in order to determine nonlinear and non-elastic bending behavior [26]. Alternatively, an inverse method for characterizing bending behavior has been proposed by Harrison et al. [24], based on an investigation of the wrinkles that develop during coupled shear-tension experiments. The bending characteristics of a preform material influence the nature of wrinkle formation during draping, which is a significant issue for the manufacture and development of complex composite structures.

### 2.2. Early draping models

The first methods for predicting fabric deformation behavior were geometric mapping-based schemes, as described by Mack and Taylor in 1956 [28]. These "fishnet" or "kinematic" models represented the fabric as a pin-jointed net, neglecting any yarn extension or slippage. Although these models were relatively simple and efficient, they did not account for mechanical phenomena such as stress, strain, or shear locking, and were restricted to simple problems without holes, bridges, or complex curves. Hence, the kinematic models were eventually replaced by more powerful forming algorithms [29]. In the 1990s, the computer animation and apparel industries investigated the use of particle-based draping models that represented fabrics as discontinuous sheets of micro-mechanical structural elements [30] with limited material properties. In spite of their aesthetic success, these particle-based methods were not appropriate for engineering applications because they neglected any technical calculations of deformation or stress. They were later replaced by continuum, discrete, and semi-discrete models.

### 2.3. Continuum methods

Continuum methods for drape modeling started as an extension of established finite-element metal-forming simulations [31]. Such macroscale modeling employs standard finite elements, usually shell or membrane elements, and assumes that the textile reinforcement acts as a homogenous sheet of material. As a result, the accuracy of continuum-based draping models primarily depends on the realism of their constitutive models and on the definition of their material properties. One limitation of this approach is that it cannot predict yarn slippage, unless such behavior is inherently defined by the material properties. In addition, out-of-plane behavior is often neglected [32,33].

A variety of constitutive models have been used in continuum methods for fabric draping, although the more effective methods tend to track and update the fiber orientations as the material deforms by using non-orthogonal or anisotropic formulations. These "updating" material behavior laws clearly show considerable improvement over the standard orthogonal methods that are built into most finite-element software packages. Two of the more successful constitutive modeling approaches for textile reinforcement materials are the hyperelastic and hypoelastic models. Hyperelastic methods can account for large deformation, anisotropy, and non-linear elasticity, so they are often used for rubbers or elastic foams that behave elastically in response to very high strains. These methods work by calculating stress from a strain energy functional, and can accurately track multiple fiber directions during textile draping. Ten Thije et al. [34] incorporated one such method, which was derived from the Helmholtz free energy theorem.

In contrast, hypoelastic models relate stress increments directly to strain increments with a constitutive tensor that contains the tensile and shear material moduli. Hypoelastic constitutive models are most effective for materials with reversible non-linear behavior and are typically used for isotropic analyses at large strains [35]. However, for fabric-draping simulations, non-orthogonal hypoelastic models have also been developed by Yu et al. [36] and Xue et al. [37]. These models have been used for various applications related to fabric draping [32,38], including mesoscale modeling of yarn behavior [35]. More recently, macroscale simulations of woven composite reinforcement materials have been developed using non-orthogonal hypoelastic continuum methods [33,39,40]. Both hyperelastic and hypoelastic constitutive models show significant improvement over the traditional Jaumann or Green-Naghdi approaches, which assume orthogonality throughout deformation [34].

### 2.4. Discrete and semi-discrete methods

Discrete and semi-discrete methods avoid macroscale homogenization of the textile reinforcement material and instead physically represent the mesoscale or microscale features of the fabric, considering the arrangement and interaction of discrete yarns or even fibers within the material. As it remains impossible to realistically simulate every fiber in each yarn for mesoscale or macroscale models, these discrete methods still require some degree of simplification and often represent yarns as beam or truss elements, using springs to simulate interactions or shear effects [41]. Recent mesoscale modeling efforts have represented yarns as a bundle of up to 48 discrete beams, in place of thousands of individual fibers [42]. This approach employs an enriched kinematic beam model, along with advanced fiber friction and contact algorithms, to better predict textile reinforcement behavior. At this scale, it is therefore possible to simulate yarn slippage, since any material continuity assumptions are restricted only to the fiber beams. However, due to computational expense, this approach is not feasible for the macroscale modeling of a full part.

In other research, yarns have been modeled within repeated unit cells (RUCs) from three-dimensional solid elements in order to predict mesoscale behavior in different textiles [43]. This method has the potential to predict yarn slippage if yarn deformation and contact interactions are appropriately defined. However, such behavior is particularly difficult to characterize, so these models remain limited to mesoscale applications and are generally used for predictive material characterization [16].

Combining aspects of these discrete methods with continuum finite-element practices has resulted in a hybrid group of semi-discrete methods, in which continuous sheets of specialized elements are used to represent textile reinforcement materials. Each specialized element is made up of a discrete number of woven RUCs [44] for greater efficiency, meaning that macroscale simulation of full parts is possible, and bending behavior can be incorporated for better wrinkle simulation [45]. For example, Allaoui et al. [46] have improved the prediction of wrinkling behavior during stamp forming, using a semi-discrete draping model that accounts for bending behavior. Instead of using stress tensors, semi-discrete methods define unit cell loading directly from yarn tension, in-plane shear, and bending. As with continuum methods, in-plane stiffness may be overestimated by the semi-discrete approach since yarn slippage is neglected. However, semi-discrete methods require less comprehensive material characterization than continuum methods and are more efficient than discrete methods. Ultimately, semi-discrete approaches are reported to be the most realistic for simulating fabric draping [47], although they are particularly complex to develop.

## 3. Infusion modeling

The main aim of resin infusion modeling is to predict fluid flow and confirm that manufacturing will be successful within the working life of the resin, without leaving dry spots or voids in the part. In addition, infusion modeling can help with the design and development of a manufacturing strategy, particularly for the location of inlets, outlets, and flow-enhancing distribution media [48].

Resin infusion through a composite reinforcement material is commonly described by Darcy's law, as shown in Eq. (1), since it is reasonable to assume that Newtonian fluids are traveling at low velocity through a porous medium:

$$v = \frac{K}{\mu} \cdot \nabla P \tag{1}$$

This equation relates the flow velocity, $v$, with the permeability, $K$, fluid viscosity, $\mu$, and overall pressure gradient through the system, $\nabla P$. Of these parameters, the fluid viscosity and pressure gradient can easily be measured or controlled in most manufacturing cases. However, fabric permeability poses a greater challenge and must be characterized either experimentally or with predictive modeling in order to effectively simulate infusion.

### 3.1. Permeability characterization

Permeability is a measure of how easily fluid flows through a porous material. For textile reinforcement materials, most infusion applications rely on anisotropic planar permeability properties; however, through-thickness permeability can also be significant in the case of thick layups. It has been reported that the transverse permeability of many preform fabrics is often one or two orders of magnitude smaller than the in-plane permeability [49], and thus has little effect on the flow through a thin layup.

Anisotropic permeability in fabrics is typically defined by two principal permeability values, $K_1$ and $K_2$, and by the principal permeability direction, $\varphi$ [50]. Despite the importance of fabric permeability in infusion modeling, and considerable research in the field [51], no standard test exists thus far for determining these properties. Current test methods exhibit considerable well-documented variability [52,53]. This variability is the result of complex flow at two different scales: viscous flow in the gaps between yarns, and capillary flow between the fibers inside each yarn [54]. The stochastic nature of woven fabrics, their susceptibility to manual handling, and ply-nesting effects are further reasons for experimental variability [55,56]. Therefore, initial attempts to benchmark permeability testing revealed that different experimental methods in different labs could vary by a whole order of magnitude for the same material [52]. Furthermore, similar methods conducted within the same lab could also result in relative standard deviations greater than ±30% [52]. However, the latest benchmarking results have shown a significant reduction in this error, as different labs using the same method were able to produce results with a relative standard deviation of ±20% [53].

#### 3.1.1. Experimental methods

Permeability characterization experiments are most often conducted to determine the in-plane properties of textile reinforcement materials, rather than the through-thickness properties. Two of the more popular in-plane characterization methods are the linear flow and radial flow experiments. Linear flow experiments monitor a linear flow front as it travels through a rectangular sample of the reinforcement material from one end to the other, while radial flow experiments trace an elliptical flow front in two dimensions from a central inlet point [50]. Either method can be conducted under saturated (pre-wetted) or unsaturated (dry) material conditions, with constant pressure or constant flow rate control. Test fluids are commonly vegetable oils, corn syrups, motor oils, or silicone oils that are representative of heated resins. Linear testing is generally considered to show better repeatability [53,57]. However, for anisotropic fabric materials, linear testing requires a greater number of tests than radial methods, which can define the anisotropic permeability properties from a single experiment.

Permeability experiments commonly rely on visual measurement methods [58]; however, thermal, electrical, and pressure measurement sensors have also been used [59]. Ahn et al. [60] studied embedded fiber optic sensors for three-dimensional permeability characterization experiments. In all cases, it is important to ensure that the test cavity is sufficiently rigid to resist any deflection that could affect flow behavior and the permeability calculations.

#### 3.1.2. Predictive modeling

Considerable research has investigated the development of predictive permeability models, in order to overcome the tedious and unreliable nature of experimental characterization methods. Initial attempts to model the permeability of porous materials were developed by Kozeny and modified by Carman [61]. The resulting Kozeny-Carman equation assumed laminar flow through a bundle of tubes, as a representation of permeation through porous material, and relied on several immeasurable parameters. Alternatively, a lubrication model to predict the permeability of UD reinforcement has been proposed [62], which assumes either square or hexagonal fiber-stacking arrangements. However, neither of these modeling approaches is strictly applicable to the real dual-scale problem, in which inter-yarn macro-pores and intra-yarn micro-pores both exist. More recently, other work has simulated flow through RUCs of the fabric architecture, with varying degrees of geometric simplification [63,64], and in one case using a lattice Boltzmann method [65]. All these methods are based on idealized yarn cross-sections and waviness. The true yarn cross-sections from textile reinforcements have also been imaged via optical coherence tomography in order to predict permeability properties [66].

Nedanov and Advani [67] and Takano et al. [68] implemented

an alternative two-step approach for permeability prediction to account for dual-scale permeability effects. Intra-yarn permeability is first calculated based on flow among the individual fibers, and then inter-yarn flow through the macro-pores is determined. The intra-yarn permeability is generally considered to be two orders of magnitude smaller than that of the fabric architecture [67], and is therefore often neglected. Other models employing voxel-based finite-difference methods [69], three-dimensional representative volume elements [70], or a reduced dimensional grid approach [12,71] have also been developed for greater efficiency. Stochastic variables such as tow spacing and ply nesting have also been investigated for textile reinforcement materials [72,73], but are not widely considered in predictive permeability models.

Although these characterization simulations are relatively rapid, they tend to oversimplify the true flow behavior through a porous textile reinforcement. Furthermore, the validity and accuracy of these methods is still reliant upon extensive experimental testing. Hence, experimental methods for permeability remain the more popular choice for cases where accuracy is essential, despite the known repeatability issues.

#### 3.1.3. Deformation dependence

Fabric deformation can have a significant effect on permeability properties; as yarns rearrange, they affect the porosity and fiber volume fraction of the material. This is not a problem in simple flat panels; however, in the manufacture of structures with complex curvature, extensive shear deformation will have a strong effect on permeability and on the subsequent flow of resin during infusion. This behavior has been widely studied; in many cases, the deformation-dependent permeability properties can change by more than 50% as a result of shearing [12,70,71,74]. Hammami et al. [74] found a four-fold increase in the anisotropy of a stitched, bi-directional, non-crimp fabric that resulted from increasing $K_1$ principal permeability values and decreasing $K_2$ values with increasing shear angles. Slade et al. [75] made similar observations for both stitched and woven fabrics. Conversely, a general reduction in both principal permeability values was recorded by Endruweit et al. [59] for various fabric architectures as shear angles increased. Further studies, both experimental and numerical, reflect similar trends of decreasing permeability with increasing shear deformation [10,64,70,76].

### 3.2. Flow simulation

Flow through porous media is commonly modeled using generalized forms of the Navier-Stokes equations and Darcy's law (Eq. (1)), including both advection and diffusion terms. Most flow models used in industry rely on a homogenous, continuum-based approximation of the preform domain, and neglect through-thickness effects, saturation, compaction, and heat transfer where possible. Early methods such as the boundary element method exhibited problems with the conservation of mass, while alternative Lagrangian finite-difference methods were limited to simple geometries [77]. A number of pure finite-element methods have also been developed with increasing sophistication, to eventually account for heat exchange, compaction, and full three-dimensional flows [78]. Alternatively, the "level set" approach has shown promising two-dimensional results [79], but has not seen a significant extension to more challenging cases. However, the most popular infusion modeling methods tend to be variations of the control volume/finite-element (CVFE) and the volume-of-fluid (VOF) methods.

#### 3.2.1. Control volume/finite-element methods

CVFE methods are common for infusion modeling as they are relatively efficient and accurate for a range of cases [49,80–83], and are able to account for merging flows and variable preform thickness. These methods simplify the infusion problem by only simulating the resin phase, neglecting the presence of any air, and using explicit integration in the time domain to solve small successive steady-state flow problems.

The flow analysis network method, which was outlined by Phelan [83] in the late 1990s, is representative of the CVFE method. With this method, the domain is discretized into elements and nodes, with independent control volumes assigned to each node, as shown in Fig. 4. The pressure gradient between the inlet and flow front is determined using the finite-element method, based on Darcy's law and on the mass continuity equation for an incompressible Newtonian fluid. The velocity field is then calculated along with the filling time of each control volume adjacent to the flow front. The shortest time to fill one of these cells is then used as the time-step for the next increment, which ensures that the flow front advances by at least one control volume. The other adjacent cells are then "partially filled," and the new numerical flow front position is determined. This method is efficient and stable, even for coarse grids, since only one differential equation must be solved [84]. However, because each time increment only aims to fill one cell, simulations with a larger number of control volumes can be slow to solve.

Bruschke and Advani [80] used an early CVFE model to model two-dimensional, isothermal, anisotropic flow through fibrous preform materials, with other researchers following suit [82]. Smoothing of the flow front has also been achieved using the method of floating imaginary nodes and elements, as described by Park and Kang [85]. In addition, Šimáček and Advani [49] were able to include artificial tow saturation modeling, using the Liquid Injection Molding Simulation software developed at the University of Delaware.

#### 3.2.2. Volume-of-fluid methods

VOF methods [86] are based on an older marker cell approach [82], which simulates a set of Lagrangian marker particles moving through a computational Eulerian mesh. These methods are ideal for the simulation of multi-phase flows, in which two or more fluid phases exist but cannot occupy the same volume. In each control volume of a VOF simulation, the volume fraction of all phases will sum to one, and a single set of governing equations is employed for all fluid phases. The governing equations for continuity, volume fraction, and momentum are shown in Eqs. (2), (3), and (4), respectively.

$$\frac{\partial \rho}{\partial t} + \nabla \cdot (\rho \boldsymbol{u}) = 0 \tag{2}$$

$$\frac{\partial}{\partial t}\left(V_{\mathrm{f},i}\rho_i\right) + \nabla \cdot \left(V_{\mathrm{f},i}\rho_i \boldsymbol{u}\right) = 0 \tag{3}$$

$$\frac{\partial (\rho \boldsymbol{u})}{\partial t} + \nabla \cdot (\rho \boldsymbol{u} \times \boldsymbol{u}) = -\nabla p + \nabla \left[\mu\left(\nabla \boldsymbol{u} + \nabla \boldsymbol{u}^{\mathrm{T}}\right)\right] + \rho g + S_K \tag{4}$$

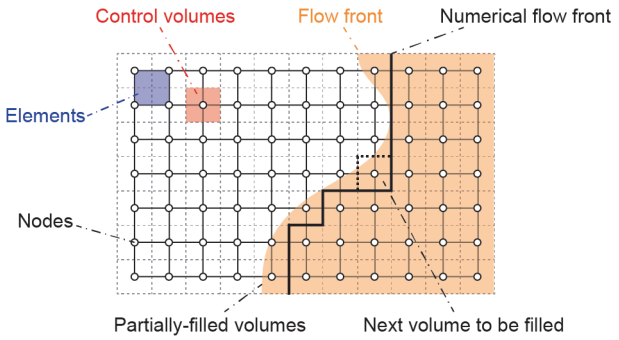


**Fig. 4.** Flow advancement in the CVFE method.

where $\boldsymbol{u}$ is the velocity vector, $p$ is pressure, $t$ is time, and $g$ is the gravitational constant. The phase-averaged density, $\rho$, and phase-averaged viscosity, $\mu$, are further defined by Eqs. (5) and (6). Here, $V_f$ is the phasic volume fraction and the subscripts $i$, r, and a relate specifically to the $i$th resin and air phases, respectively.

$$\rho = V_{f,r}\rho_r + \left(1 - V_{f,r}\right)\rho_a \tag{5}$$

$$\mu = V_{f,r}\mu_r + \left(1 - V_{f,r}\right)\mu_a \tag{6}$$

In Eq. (7), the source term, $S_K$, is related to the flow resistance of a porous material, and is reflective of Darcy's law from Eq. (1).

$$S_K = -\frac{\mu}{K}\boldsymbol{u} \tag{7}$$

Because this approach solves the set of partial differential equations simultaneously, it can suffer from convergence issues if the mesh and time discretization are not carefully established. However, the VOF method is very effective at simulating regions with significant differences in permeability characteristics, such as open channels, which are not solvable using CVFE methods [84].

### 3.3. Other considerations

In addition to the essential modeling factors that affect resin flow behavior (permeability, pressure, viscosity, and inlet/outlet location), there are a number of further considerations for improved flow modeling. Since the properties of textile reinforcement materials are inherently variable and are susceptible to handling and cutting, probabilistic tools that can predict and account for possible flow disturbances have been developed [87]. Given that race-tracking effects at edges or joints can significantly influence flow behavior, it is particularly important that any given infusion strategy be tolerant of their occurrence.

Passive controls such as additional outlets, which are closed off as resin fills past them, and flow-enhancing material, which is common for vacuum-assisted resin infusion processes, have also been investigated. When modeled, passive controls can add significant complexity to the optimization of an infusion strategy; therefore, advanced algorithms have been used to better predict the optimal shape and location of flow-enhancing media [88]. Exhaustive "brute force" approaches for optimizing inlet and outlet locations can be prohibitively time-consuming when there are a large number of variables. Hence, more sophisticated methods, such as the use of centroidal Voronoi diagrams [89], have been demonstrated to greatly reduce the number of simulation iterations required for effective optimization. Active flow-control measures have also been studied, for example, using live pressure or flow rate control at different inlet locations across the part [90]. However, it is evident that such measures further complicate predictive modeling, as suitable locations for additional sensors and variable flow inlets must be considered.

Through-thickness effects, tool compaction, and void formation can all be significant issues during infusion. For many thin composite components, through-thickness effects and tool compaction are often neglected. However, for thicker layups, an accurate prediction of three-dimensional flow and of tool compaction can become necessary. Tool compaction is particularly important for processes that rely on flexible tooling, which can deform under increasing internal mold pressure as a result of resin infiltration [91,92]. For example, the effect of dry and wet compaction during infusion has been investigated for a chopped-strand mat reinforcement and simulated using a one-dimensional Galerkin finite-element method [93]. Mesoscale mechanical modeling of compaction behavior has also reported good agreement with experimental testing [94]. The formation and transportation of voids is common during infusion and can have a significant effect on the preform saturation and ultimate part performance [95]. Recent work has investigated the use of a dimensionless "modified capillary number" to predict void formation, bubble compression, and transport at the resin flow front, based on the ratio of viscous force and surface tension [54].

## 4. Process modeling

The complete simulation of resin infusion manufacturing is challenging because it should account for the mechanical behavior of the preform, the flow of resin through the deformed material, and even the curing behavior in some cases. This is further complicated by deformation-dependent permeability properties, saturation, and void creation. In addition, for processes that employ flexible tooling, considerable compaction effects may affect filling behavior during infusion.

Due to these challenges, it is very difficult to create a model that can account for all the necessary effects. However, researchers are starting to develop models that can account for some of these multidisciplinary effects. Such models can result in considerable improvement over traditional simulations, which consider forming and infusion as completely independent processes.

The concept of an "integrated design tool" that can predict the full manufacturing process and final part performance has been prominently proposed by Lomov et al. [11] and Verleye et al. [12] for over 15 years. Recent work accounts for the effect of fabric deformation on infusion behavior and includes considerations for saturation effects [96,97]. However, such process-modeling efforts have only very recently seen full-scale experimental validation [98], as highlighted in the following sections of this paper.

## 5. Demonstration of a multi-physics process model

A multi-physics process model that more realistically predicts fabric deformation and resin flow during vacuum-assisted resin infusion processes has been developed. This process model integrates a range of characterization testing and numerical models, as shown in Fig. 5 [98], to achieve this goal. The basis of this model is a continuum draping model, which is first employed in ABAQUS® to predict fabric deformation. The results of this model are then passed on to an ANSYS Fluent® infusion model, for the prediction of resin flow through the deformed reinforcement material. The accuracy of the draping model relies on the characterization of fabric tensile and shear properties, although deformation-dependent permeability properties are also needed, in combination with the draping results,

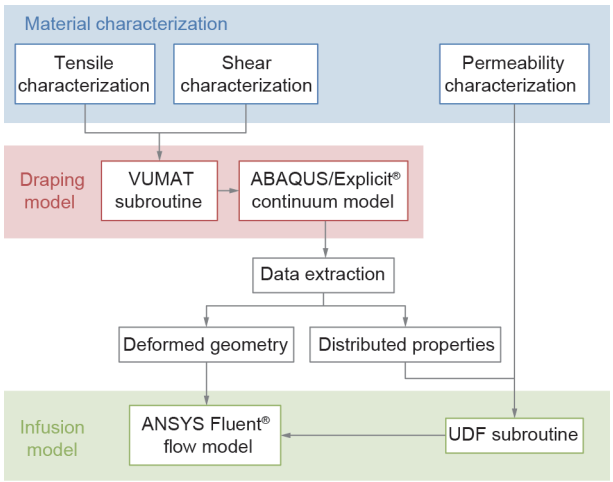


**Fig. 5.** Workings of the multi-physics process model [98]. UDF: user-defined function.

to support the infusion model. An explicit user-defined subroutine (e.g., VUMAT subroutine in ABAQUS/Explicit®) defines the draping material model and incorporates the material properties, in order to realistically track non-orthogonal yarn rotations. Similarly, a user-defined function (UDF) subroutine is used to assign variable permeability properties across the infusion domain in the ANSYS Fluent® flow model. The complete details of this multi-physics process model can be found in the literature [98]; however, the following sections highlight its novel application and validation against full-scale experimental forming and infusion trials.

### 5.1. Full-scale experiments

In order to assess the validity of the multi-physics process model, vacuum infusion experiments were conducted over a large "double dome" tool. This common complex geometry for forming studies is well-documented in the literature [33,40]. The male tool was constructed from structural foam, coated, and recessed 120 mm deep into an outer frame with the dimensions 950 mm × 550 mm. The outer frame, which was the same height as the double dome tool, allowed for better bag conformity and prevented wrinkling, compared with a basic bagging approach directly over the top of the mold.

Single plies of the dry, plain-weave carbon fiber material were cut to 800 mm × 500 mm, with either 0°/90° or –45°/45° yarn orientations. These were then marked with a 50 mm silver grid to support optical measurements throughout the forming and infusion phases. The preform material was placed over the mold and underneath a vacuum bag, along with three vacuum ports and some additional distribution media (Fig. 6) [98]. The bag was sealed at the frame edges and the central vacuum port was connected to the vacuum pump to commence the forming process. Once the bag and fabric material were drawn to the bottom of the mold, secondary vacuum ports at the long ends of the mold were connected to the vacuum pump and the central port was closed off. Conformity of the bag and fabric reinforcement material was checked thoroughly to remedy any bridging in the concave regions of the tool.

For infusion, the central port was then connected to an oil reservoir and opened to initiate fluid flow. Olive oil was used as the representative test fluid, as it has a standard room temperature viscosity of 0.084 Pa·s that was consistent with typical infusion resin viscosities (between 0.001 Pa·s and 0.3 Pa·s) [8]. During testing, a number of images were taken at regular intervals to record the flow behavior through each sample. Both the forming and infusion stages of the full-scale demonstration experiments are visually described in Fig. 6.

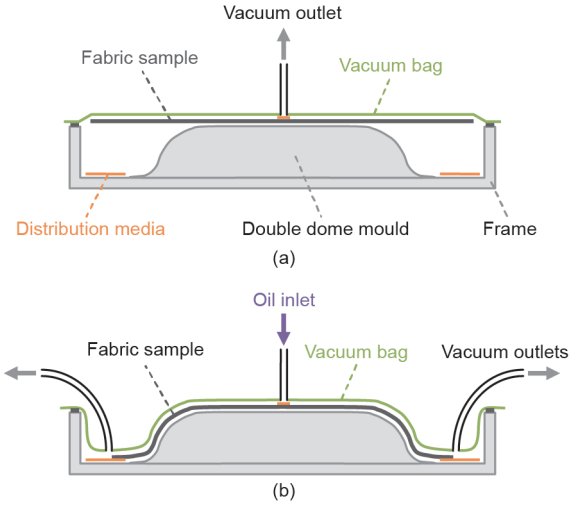


**Fig. 6.** The two-stage experimental process [98]. (a) Forming; (b) infusion.

### 5.2. Draping model

A continuum-based draping model was employed in ABAQUS/Explicit® for a typical double dome part, similar to work by Khan et al. [33] and Peng and Rehman [40]. A single fabric layer was represented as a continuous sheet of membrane elements, while a custom VUMAT material subroutine provided the hypoelastic material model. This subroutine was designed to track the true, non-orthogonal yarn orientations throughout the forming process, and to calculate the material response based on experimentally characterized tensile and shear properties ($E$ and $G_{12}$). The development and implementation of this subroutine is well documented in the literature [99]. Bending effects were neglected for the purposes of this investigation.

The fabric tensile properties were determined from uniaxial strip testing according to the standard ASTM D5035-11 [19] for a dry carbon plain-weave fabric with 3K tows and an areal density of 0.193 kg·m$^{-2}$. A near-linear elastic response was recorded, resulting in a tensile modulus, $E$, of 15 GPa.

Bias extension testing was conducted to characterize the shear behavior of the plain-weave fabric, using DIC for enhanced strain measurement. Full details of this testing have been published previously [100]. An exponential function was found to best fit the highly non-linear shear response. Hence, Eq. (8) was used to describe the shear modulus, $G_{12}$, of the fabric, thus capturing both the relative freedom of yarn rotation at low shear angles and the significant shear-locking behavior.

$$G_{12} = 8.916\times10^{-3}\,e^{4.24\gamma} + 1.056\times10^{-11}\,e^{23.69\gamma}\ \text{MPa} \tag{8}$$

where e is Euler's number and $\gamma$ is shear angle. The deformable fabric sheet was modeled in quarter symmetry with around 1000 M3D4R elements, at a thickness of 0.4 mm for both 0°/90° and –45°/45° cases. The fabric sheet was first held in place between a rigid blank holder and a double dome die, before a matching rigid punch was used to form the material. All rigid parts were simulated with a slightly finer mesh of R3D3 elements. The global contact condition for friction was set at 0.15, following a parametric investigation consistent with general practice [33,39,40].

Since the results from the ABAQUS® draping model were incompatible with those from the ANSYS Fluent® model, a Python script was used to automatically generate two more compatible independent files, which contained the "deformed geometry" information and the "distributed properties" data, respectively.

### 5.3. Infusion model

As this modeling demonstration focused on the significance of deformation-dependent permeability behavior, isothermal conditions were assumed, while saturation and compaction effects were largely neglected. For flexibility and reliability, ANSYS Fluent® was used for the infusion model, essentially employing an Eulerian VOF method. Hence, both the resin and air phases were traced throughout the domain during infusion as interpenetrating continua.

In support of the infusion model, permeability tests were conducted using unsaturated radial flow experiments for a range of fabric shear deformation (0°–40°). Full details of the experimental method and permeability calculations can be found in previous work [101]. The resulting permeability properties showed $K_1$ values to increase and $K_2$ values to generally decrease with increasing shear angle; hence, the combined effect of $K_1$ increasing and $K_2$ decreasing leads directly to a great increase in anisotropy. However, because the permeability tests were conducted between rigid plates, while the full-scale experiments were under bagging film, further calibration was required. Constant calibration factors of 0.667 and 0.5 were

applied to $K_1$ values and $K_2$ values, respectively, over the full range of shear angles and across all modeling efforts with different material orientations, based on experimental observations. The polynomial permeability curves for infusion modeling were defined by Eqs. (9) and (10). The principal permeability direction, $\varphi$, was simulated using Eq. (11) and transitions from an initial alignment with the weft yarn direction to alignment with the fabric bias direction at higher shear angles.

$$K_1 = 0.667(-6.641\gamma^4 + 13.28\gamma^3 - 8.414\gamma^2 + 2.4\gamma + 0.6028)\times 10^{-10}\ \mathrm{m}^2 \quad (9)$$

$$K_2 = 0.5(-7.7\gamma^4 + 14.66\gamma^3 - 9.261\gamma^2 + 1.605\gamma + 0.5313)\times 10^{-10}\ \mathrm{m}^2 \quad (10)$$

$$\varphi = \begin{cases} \dfrac{|\gamma|}{20^\circ}\left(45^\circ - \dfrac{|\gamma|}{2}\right) & \text{if } |\gamma| \le 20^\circ \\ 45^\circ - \dfrac{|\gamma|}{2} & \text{if } |\gamma| > 20^\circ \end{cases} \quad (11)$$

The infusion domain was re-modeled in the ANSYS software suite using nodal position data from the "deformed geometry" file, which resulted from the draping simulation. The quarter symmetry and a domain thickness of 0.4 mm were maintained, while the new mesh consisted of around 1000 elements. A 50 mm diameter region was partitioned from the domain in order to better represent the inlet conditions. Free-slip (symmetric) boundary conditions were applied to all the domain walls, aside from the inlet and a single outlet, as shown in Fig. 7 [98]. The inlet and outlet pressure were 101.3 kPa and 0.3 kPa, respectively, while the undeformed baseline material porosity was 0.724. The oil viscosity for the 0°/90° and –45°/45° orientation cases was 0.0756 Pa·s and 0.0993 Pa·s, respectively, based on measured viscosity-temperature curves.

Upon initialization of the model, a UDF subroutine was employed to collect and store all the information from the "distributed properties" file, converting local shear angles into local permeability information based on Eqs. (9)–(11). These properties were then assigned on a cell-by-cell basis, resulting in a complex map of the flow characteristics based on the original shear deformation, as shown in Fig. 7.

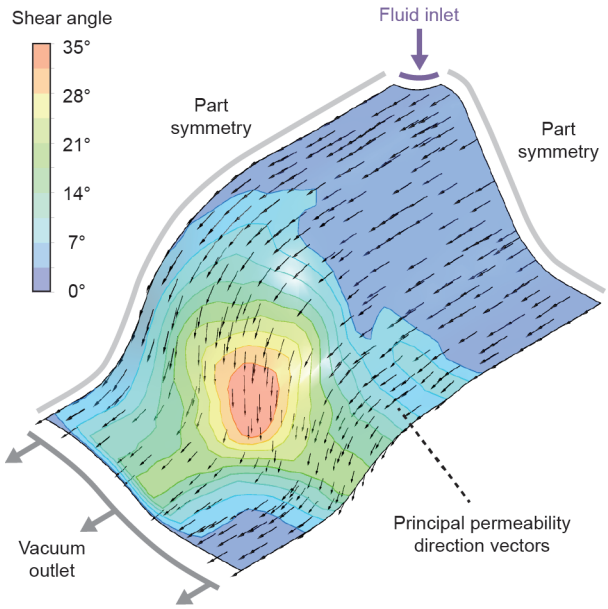


**Fig. 7.** Deformation-dependent permeability properties defined across the 0°/90° orientation model [98].

### 5.4. Results

#### 5.4.1. Draping

The plain-weave material formed well to the mold for repeated tests of different samples in each orientation, without any signs of wrinkling. Good symmetry was observed among the four quadrants of each test, with only minor fraying at the sample edges (Fig. 8) [98]. Grid point locations from each of the four quadrants of each test were averaged and compared against the simulated draping results. The predicted grid locations were subsequently found to have less than 2% error from the mean experimental results.

Furthermore, shear angles were evaluated at a number of locations across each quadrant of symmetry, as indicated in Fig. 8, for comparison with the draping simulation results. Experimental shear angle values for the 0°/90° orientation samples were seen to vary from 0° to 36° with very little variation. For the –45°/45° orientation samples, experimental shear angles ranged from –24° to 15°. There was ultimately very good agreement between the experimental and modeled results, as can be seen in Fig. 9 [98] for both the 0°/90° and –45°/45° orientation cases.

#### 5.4.2. Infusion

The experimental infusion was quite repeatable in both fabric orientations, with no indication of race-tracking behavior. In order to better demonstrate the benefits of the multi-physics process model, which accounts for deformation-dependent permeability properties, a traditional isotropic infusion model was also executed under similar conditions. Isotropic and homogenous permeability properties were applied across the infusion domain based on the calibrated mean $K_1$ and $K_2$ values from experimental permeability characterization ($K_1 = K_2 = 3.3 \times 10^{-11}$ m$^2$). The experimental and modeled flow fronts for 0°/90° and –45°/45° orientation samples are shown in Fig. 10 and Fig. 11 [98], respectively (at 1255 s and 850 s). The modeled flow front is taken as the contour line for a 0.5 phasic volume fraction of oil and air, as is experimentally validated in the literature [98]. In each case, there was quite good agreement

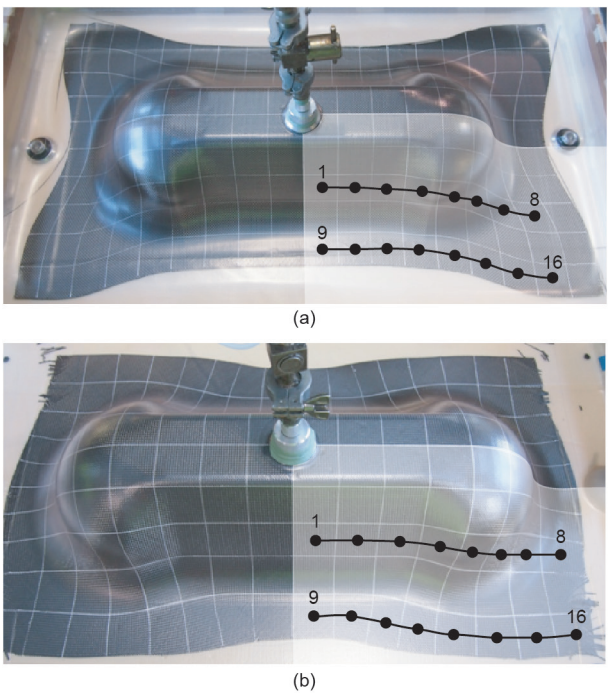


**Fig. 8.** Formed double dome samples, with shear measurement locations representative of each quadrant of symmetry [98]. (a) 0°/90° orientation; (b) –45°/45° orentation.

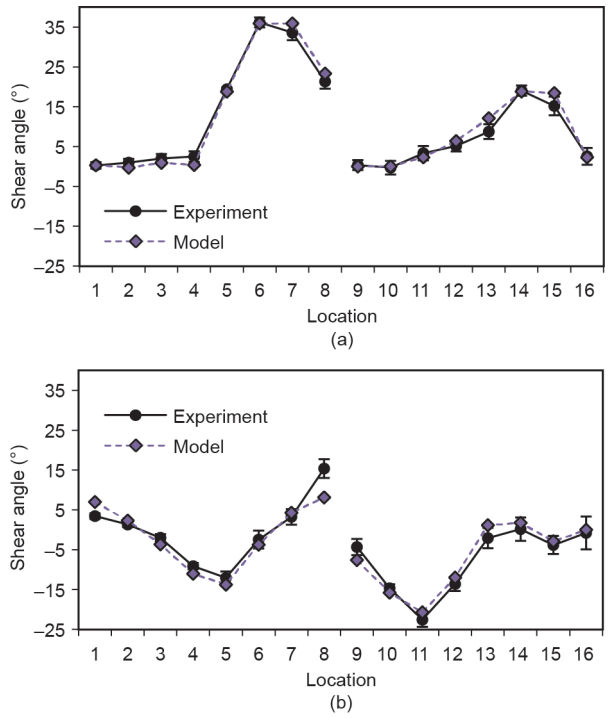


**Fig. 9.** Comparison of experimental and modeled shear measurements across 16 locations in each sample orientation [98]. (a) 0°/90° orientation; (b) –45°/45° orientation.

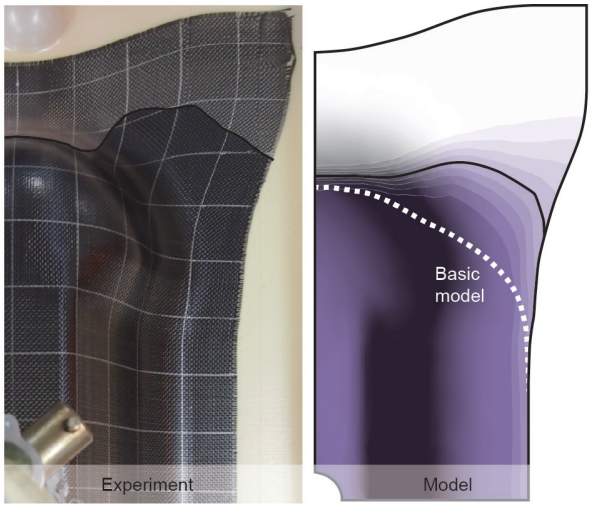


**Fig. 10.** Flow front comparison at 1255 s for 0°/90° orientation sample [98].

between the multi-physics model and the experimental results, while the basic model was unable to capture the enhanced flow resulting from local shearing. The anisotropic behavior in regions of high shear deformation has been clearly captured in Fig. 10.

It is notable that the photographed flow in Fig. 10 and Fig. 11 includes some perspective distortion that was introduced by a wide-angle camera lens, particularly for the raised region of the dome. However, since the exact double dome geometry and grid dimensions were known, the true flow front location for each test was easily calculated. Hence, a more accurate comparison of the experimental multi-physics model and the basic model results can be seen in Fig. 12 and Fig. 13 [98] for each orientation case at various filling times. These results show the improvement of the multi-physics approach over a basic model, although the more advanced simulation still showed some variation from the experimental results.

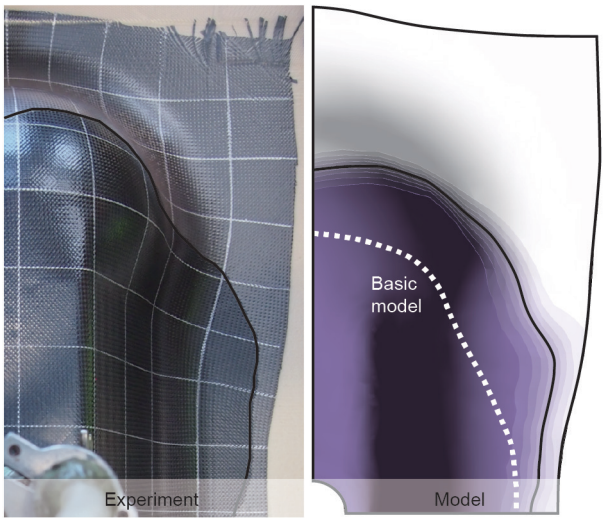


**Fig. 11.** Flow front comparison at 850 s for –45°/45° orientation sample [98].

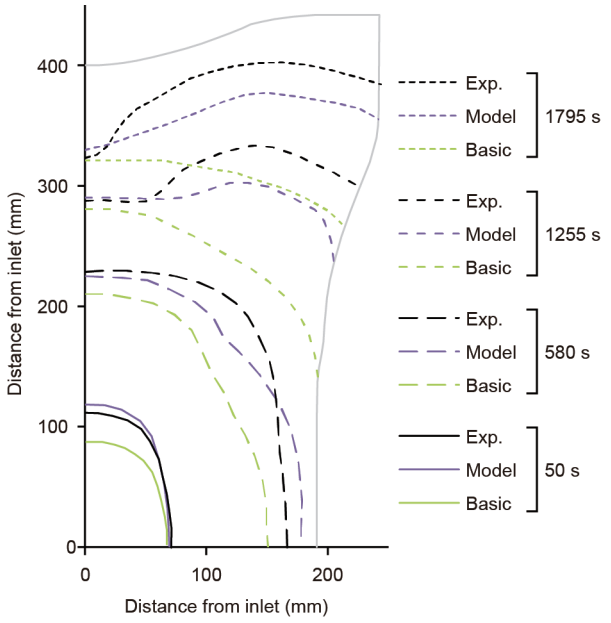


**Fig. 12.** Experimental and modeled flow front progression through the 0°/90° orientation sample [98].

## 6. Conclusions

Growing demand for larger and more complex aerostructures is encouraging the adoption of out-of-autoclave manufacturing techniques for textile-reinforced composites. Process modeling is simultaneously becoming a sophisticated alternative to traditional part-development methods, allowing for significant time and cost reductions. Such modeling is increasingly reliant on multi-physics simulations that couple models from a variety of disciplines. In the case of resin infusion manufacturing with textile reinforcement materials, the physical draping of the fabric and the subsequent resin flow through the material are the key stages of the process. In order to predict these accurately, a range of methods at different scales have been reported. Although considerable work has been done to investigate the characterization of material properties in order to support modeling efforts, further research and standardization is still required before process modeling can fully account for the multi-scale behavior of textile reinforcement materials.

A recent multi-physics process model showed considerable

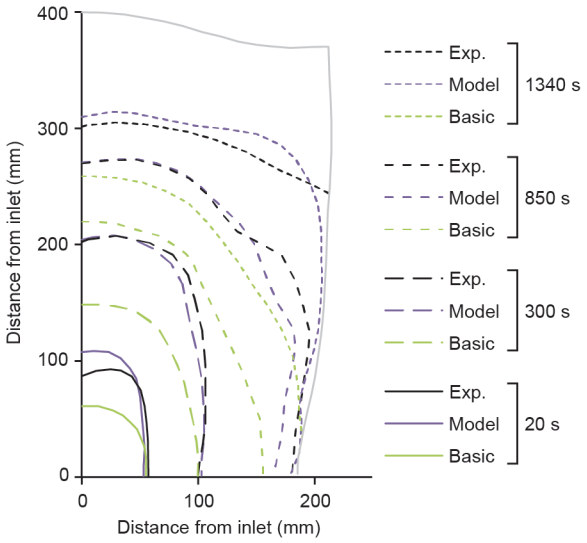


**Fig. 13.** Experimental and modeled flow front progression through the –45°/45° orientation sample [98].

improvement over the traditional modeling approach. By accounting for the effect of deformation on permeability properties, this advanced model was able to better predict experimental flow behavior in a full-scale double dome infusion. However, some variance was still observed between the simulation and experimental results, which was probably a result of inaccurate permeability properties and of compaction effects that were neglected by the model. In this case, single-ply testing provided a novel demonstration of the model's capability to capture realistic flow behavior. However, for greater industrial impact, future work with multiple-ply applications should be considered.

## Acknowledgements

This research was originally supported under the Australian Research Council's Linkage Projects funding scheme (LP100100508) at Monash University in partnership with Boeing Research & Technology Australia. The second author would also like to acknowledge the financial support of Bombardier and the Royal Academy of Engineering.

## Compliance with ethics guidelines

Robert S. Pierce and Brian G. Falzon declare that they have no conflict of interest or financial conflicts to disclose.

## References

[1] EADS Deutschland GmbH, Corporate Research Center. The research requirements of the transport sectors to facilitate an increased usage of composite materials. Part I : The composite material research requirements of the aerospace industry. Report. Munchen: EADS Deutschland GmbH, Corporate Research Center. 2004 Jun. Contract No.: G4RT-CT-2001-05054.
[2] Soutis C. Fibre reinforced composites in aircraft construction. Prog Aerosp Sci 2005;41(2):143–51.
[3] Deo R, Starnes J, Holzwart R. Low-cost composite materials and structures for aircraft applications. Report. Hampton: NASA Langley Research Center; 2003 Oct. Report No.: 20030097981.
[4] Roeseler WG, Sarh B, Kismarton MU. Composite structures: The first 100 years. In: Proceedings of the 16th International Conference on Composite Materials; 2007 Jul 9; Kyoto, Japan; 2007. p. 1–10.
[5] Gardiner G. Resin-infused MS-21 wings and wingbox. High Performance Composites 2014;22(1):29.
[6] Poe CC, Dexter HB, Raju IS. Review of the NASA textile composites research. J Aircr 1999;36(5):876–84.
[7] Adumitroaie A, Barbero EJ. Beyond plain weave fabrics—II. Mechanical properties. Compos Struct 2011;93(5):1449–62.
[8] Williams C, Summerscales J, Grove S. Resin infusion under flexible tooling (RIFT): A review. Compos Part A Appl Sci Manuf 1996;27(7):517–24.
[9] Long AC, editor. Composites forming technologies. Cambridge: Woodhead Publishing; 2007.
[10] Smith P, Rudd CD, Long AC. The effect of shear deformation on the processing and mechanical properties of aligned reinforcements. Compos Sci Technol 1997;57(3):327–44.
[11] Lomov SV, Huysmans G, Luo Y, Parnas RS, Prodromou A, Verpoest I, et al. Textile composites: Modeling strategies. Compos Part A Appl Sci Manuf 2001;32(10):1379–94.
[12] Verleye B, Lomov SV, Long A, Verpoest I, Roose D. Permeability prediction for the meso-macro coupling in the simulation of the impregnation stage of resin transfer moulding. Compos Part A Appl Sci Manuf 2010;41(1):29–35.
[13] Wang J, Page JR, Paton R. Experimental investigation of the draping properties of reinforcement fabrics. Compos Sci Technol 1998;58(2):229–37.
[14] Flores FG, Oñate E. Applications of a rotation-free triangular element for finite strain analysis of thin shells and membranes. In: Oñate E, Kröplin B, editors Textile composites and inflatable structures. Dordrecht: Springer; 2005. p. 69–88.
[15] Ten Thije RHW, Akkerman R. A multi-layer triangular membrane finite element for the forming simulation of laminated composites. Compos Part A Appl Sci Manuf 2009;40(6–7):739–53.
[16] Boisse P, Gasser A, Hivet G. Analyses of fabric tensile behaviour: Determination of the biaxial tension-strain surfaces and their use in forming simulations. Compos Part A Appl Sci Manuf 2001;32(10):1395–414.
[17] Gasser A, Boisse P, Hanklar S. Mechanical behaviour of dry fabric reinforcements. 3D simulations versus biaxial tests. Comput Mater Sci 2000;17(1):7–20.
[18] Boisse P, Zouari B, Daniel JL. Importance of in-plane shear rigidity in finite element analyses of woven fabric composite preforming. Compos Part A Appl Sci Manuf 2006;37(12):2201–12.
[19] ASTM International. ASTM D5035-11 Standard test method for breaking force and elongation of textile fabrics (strip method). West Conshohocken: ASTM International; 2015.
[20] Kawabata S. The standardization and analysis of hand evaluation. Osaka: Osaka Tiger Printing Co., Ltd; 1980.
[21] Potluri P, Perez Ciurezu DA, Ramgulam RB. Measurement of meso-scale shear deformations for modeling textile composites. Compos Part A Appl Sci Manuf 2006;37(2):303–14.
[22] Culpin MF. The shearing of fabrics: A novel approach. J Textil Inst 1979;70(3):81–8.
[23] Harrison P, Clifford MJ, Long AC. Shear characterization of viscous woven textile composites: A comparison between picture frame and bias extension experiments. Compos Sci Technol 2004;64(10–11):1453–65.
[24] Harrison P, Abdiwi F, Guo Z, Potluri P, Yu WR. Characterising the shear-tension coupling and wrinkling behaviour of woven engineering fabrics. Compos Part A Appl Sci Manuf 2012;43(6):903–14.
[25] Cao J, Akkerman R, Boisse P, Chen J, Cheng HS, de Graaf EF, et al. Characterization of mechanical behavior of woven fabrics: Experimental methods and benchmark results. Compos Part A Appl Sci Manuf 2008;39(6):1037–53.
[26] De Bilbao E, Soulat D, Hivet G. Experimental study of bending behaviour of reinforcements. Exp Mech 2009;50(3):333–51.
[27] Syerko E, Comas-Cardona S, Binetruy C. Models of mechanical properties/behavior of dry fibrous materials at various scales in bending and tension: A review. Compos Part A Appl Sci Manuf 2012;43(8):1365–88.
[28] Mack C, Taylor HM. The fitting of woven cloth to surfaces. J Textil Inst Trans 1956;47(9):T477–88.
[29] Van Der Weeën F. Algorithms for draping fabrics on doubly-curved surfaces. Int J Numer Methods Eng 1991;31(7):1415–26.
[30] Breen DE, House DH, Wozny MJ. Predicting the drape of woven cloth using interacting particles. In: Proceedings of the 21st Annual Conference on Computer Graphics and Interactive Techniques; 1994 Jul 24–29; Orlando, USA. New York: ACM; 1994. p. 365–72.
[31] Dong L, Lekakou C, Bader MG. Processing of composites: Simulations of the draping of fabrics with updated material behaviour law. J Compos Mater 2001;35(2):138–63.
[32] Peng XQ, Cao J. A continuum mechanics-based non-orthogonal constitutive model for woven composite fabrics. Compos Part A Appl Sci Manuf 2005;36(6):859–74.
[33] Khan MA, Mabrouki T, Vidal-Sallé E, Boisse P. Numerical and experimental analyses of woven composite reinforcement forming using a hypoelastic behaviour. Application to the double dome benchmark. J Mater Process Technol 2010;210(2):378–88.
[34] Ten Thije RHW, Akkerman R, Huétink J. Large deformation simulation of anisotropic material using an updated Lagrangian finite element method. Comput Methods Appl Mech Eng 2007;196(33–34):3141–50.
[35] Badel P, Gauthier S, Vidal-Sallé E, Boisse P. Rate constitutive equations for computational analyses of textile composite reinforcement mechanical behaviour during forming. Compos Part A Appl Sci Manuf 2009;40(8):997–1007.
[36] Yu WR, Pourboghrat F, Chung K, Zampaloni M, Kang TJ. Non-orthogonal constitutive equation for woven fabric reinforced thermoplastic composites. Compos Part A Appl Sci Manuf 2002;33(8):1095–105.
[37] Xue P, Peng X, Cao J. A non-orthogonal constitutive model for characterizing woven composites. Compos Part A Appl Sci Manuf 2003;34(2):183–93.
[38] Yu WR, Harrison P, Long A. Finite element forming simulation for non-crimp fabrics using a non-orthogonal constitutive equation. Compos Part A Appl Sci Manuf 2005;36(8):1079–93.
[39] Peng X, Ding F. Validation of a non-orthogonal constitutive model for woven composite fabrics via hemispherical stamping simulation. Compos Part A Appl

Sci Manuf 2011;42(4):400–7.
[40] Peng X, Rehman ZU. Textile composite double dome stamping simulation using a non-orthogonal constitutive model. Compos Sci Technol 2011;71(8):1075–81.
[41] Jauffrès D, Sherwood JA, Morris CD, Chen J. Discrete mesoscopic modeling for the simulation of woven-fabric reinforcement forming. Int J Mater Form 2010;3(Suppl 2):1205–16.
[42] Durville D. Simulation of the mechanical behaviour of woven fabrics at the scale of fibers. Int J Mater Form 2010;3(Suppl 2):1241–51.
[43] Badel P, Vidal-Sallé E, Boisse P. Computational determination of in-plane shear mechanical behaviour of textile composite reinforcements. Comput Mater Sci 2007;40(4):439–48.
[44] Hamila N, Boisse P. A meso-macro three node finite element for draping of textile composite preforms. Appl Compos Mater 2007;14(4):235–50.
[45] Hamila N, Boisse P, Sabourin F, Brunet M. A semi-discrete shell finite element for textile composite reinforcement forming simulation. Int J Numer Methods Eng 2009;79(12):1443–66.
[46] Allaoui S, Boisse P, Chatel S, Hamila N, Hivet G, Soulat D, et al. Experimental and numerical analyses of textile reinforcement forming of a tetrahedral shape. Compos Part A Appl Sci Manuf 2011;42(6):612–22.
[47] Boisse P, Aimène Y, Dogui A, Dridi S, Gatouillat S, Hamila N, et al. Hypoelastic, hyperelastic, discrete and semi-discrete approaches for textile composite reinforcement forming. Int J Mater Form 2010;3(Suppl 2):1229–40.
[48] Advani SG, Simacek P. Liquid composite molding: Role of modeling and simulation in process advancement. In: Proceeding of the 20th International Conference on Composite Materials; 2015 Jul 19–24; Copenhagen: Denmark; 2015.
[49] Šimáček P, Advani SG. Desirable features in mold filling simulations for liquid composite molding processes. Polym Compos 2004;25(4):355–67.
[50] Weitzenböck JR, Shenoi RA, Wilson PA. Radial flow permeability measurement. Part A: Theory. Compos Part A Appl Sci Manuf 1999;30(6):781–96.
[51] Sharma S, Siginer DA. Permeability measurement methods in porous media of fiber reinforced composites. Appl Mech Rev 2010;63(2):020802.
[52] Arbter R, Beraud JM, Binetruy C, Bizet L, Bréard J, Comas-Cardona S, et al. Experimental determination of the permeability of textiles: A benchmark exercise. Compos Part A Appl Sci Manuf 2011;42(9):1157–68.
[53] Vernet N, Ruiz E, Advani S, Alms JB, Aubert M, Barburski M, et al. Experimental determination of the permeability of engineering textiles: Benchmark II. Compos Part A Appl Sci Manuf 2014;61:172–84.
[54] Park CH, Lebel A, Saouab A, Bréard J, Lee W. Modeling and simulation of voids and saturation in liquid composite molding processes. Compos Part A Appl Sci Manuf 2011;42(6):658–68.
[55] Hoes K, Dinescu D, Sol H, Parnas RS, Lomov S. Study of nesting induced scatter of permeability values in layered reinforcement fabrics. Compos Part A Appl Sci Manuf 2004;35(12):1407–18.
[56] Endruweit A, Long AC. Influence of stochastic variations in the fiber spacing on the permeability of bi-directional textile fabrics. Compos Part A Appl Sci Manuf 2006;37(5):679–94.
[57] Lundström TS, Stenberg R, Bergström R, Partanen H, Birkeland PA. In-plane permeability measurements: A nordic round-robin study. Compos Part A Appl Sci Manuf 2000;31(1):29–43.
[58] Luo Y, Verpoest I, Hoes K, Vanheule M, Sol H, Cardon A. Permeability measurement of textile reinforcements with several test fluids. Compos Part A Appl Sci Manuf 2001;32(10):1497–504.
[59] Endruweit A, McGregor P, Long AC, Johnson MS. Influence of the fabric architecture on the variations in experimentally determined in-plane permeability values. Compos Sci Technol 2006;66(11–12):1778–92.
[60] Ahn SH, Lee WI, Springer GS. Measurement of the three-dimensional permeability of fiber preforms using embedded fiber optic sensors. J Compos Mater 1995;29(6):714–33.
[61] Carman PC. Flow of gases through porous media. New York: Academic Press; 1956.
[62] Gebart BR. Permeability of unidirectional reinforcements for RTM. J Compos Mater 1992;26(8):1100–33.
[63] Yu B, Lee LJ. A simplified in-plane permeability model for textile fabrics. Polym Compos 2000;21(5):660–85.
[64] Dungan FD, Senoguz MT, Sastry AM, Faillaci DA. Simulations and experiments on low-pressure permeation of fabrics: Part I—3D modeling of unbalanced fabric. J Compos Mater 2001;35(14):1250–84.
[65] Belov EB, Lomov SV, Verpoest I, Peters T, Roose D, Parnas RS, et al. Modeling of permeability of textile reinforcements: Lattice Boltzmann method. Compos Sci Technol 2004;64(7–8):1069–80.
[66] Dunkers JP, Phelan FR, Zimba CG, Fly KM, Sanders DP, et al. The prediction of permeability for an epoxy/E-glass compsoite using optical coherence tomographic images. Polym Compos 2001;22(6):803–14.
[67] Nedanov PB, Advani SG. Numerical computation of the fiber preform permeability tensor by the homogenization method. Polym Compos 2002;23(5):758–70.
[68] Takano N, Zako M, Okazaki T, Terada K. Microstructure-based evaluation of the influence of woven architecture on permeability by asymptotic homogenization theory. Compos Sci Technol 2002;62(10–11):1347–56.
[69] Verleye B, Croce R, Griebel M, Klitz M, Lomov SV, Morren G, et al. Permeability of textile reinforcements: Simulation, influence of shear and validation. Compos Sci Technol 2008;68(13):2804–10.
[70] Loix F, Badel P, Orgéas L, Geindreau C, Boisse P. Woven fabric permeability: From textile deformation to fluid flow mesoscale simulations. Compos Sci Technol 2008;68(7–8):1624–30.
[71] Wong CC, Long AC, Sherburn M, Robitaille F, Harrison P, Rudd CD. Comparisons of novel and efficient approaches for permeability prediction based on the fabric architecture. Compos Part A Appl Sci Manuf 2006;37(6):847–57.
[72] Lomov SV, Verpoest I, Peeters T, Roose D, Zako M. Nesting in textile laminates: Geometrical modeling of the laminate. Compos Sci Technol 2003;63(7):993–1007.
[73] Vanaerschot A, Cox BN, Lomov SV, Vandepitte D. Stochastic multi-scale modeling of textile composites based on internal geometry variability. Comput Struc 2013;122:55–64.
[74] Hammami A, Trochu F, Gauvin R, Wirth S. Directional permeability measurement of deformed reinforcement. J Reinf Plast Compos 1996;15(6):552–62..
[75] Slade J, Sozer EM, Advani SG. Fluid impregnation of deformed preforms. J Reinf Plast Compos 2000;19(7):552–68.
[76] Lai CL, Young WB. Model resin permeation of fiber reinforcements after shear deformation. Polym Compos 1997;18(5):642–8.
[77] Trochu F, Gauvin R. Limitations of a boundary-fitted finite difference method for the simulation of the resin transfer molding proccess. J Reinf Plast Compos 1992;11(7):772–86.
[78] Trochu F, Ruiz E, Achim V, Soukane S. Advanced numerical simulation of liquid composite molding for process analysis and optimization. Compos Part A Appl Sci Manuf 2006;37(6):890–902.
[79] Soukane S, Trochu F. Application of the level set method to the simulation of resin transfer molding. Compos Sci Technol 2006;66(7–8):1067–80.
[80] Bruschke MV, Advani SG. A finite element/control volume approach to mold filling in anisotropic porous media. Polym Compos 1990;11(6):398–405.
[81] Kang MK, Lee WI, Hahn HT. Analysis of vacuum bag resin transfer molding process. Compos Part A Appl Sci Manuf 2001;32(11):1553–60.
[82] Ngo ND, Mohan RV, Chung PW, Tamma KK, Shires DR. Recent developments encompassing non-isothermal/isothermal liquid composite molding process modeling/analysis: Physically accurate, computationally effective, and affordable simulations and validations. J Thermoplast Compos Mater 1998;11(6):493–532.
[83] Phelan FR. Simulation of the injection process in resin transfer molding. Polym Compos 1997;18(4):460–76.
[84] Luz FF, Amico SC, Souza JÁ, Barbosa ES, Barbosa de Lima AG. Resin transfer molding process: Fundamentals, numerical computation and experiments. In: Delgado JMPQ, Barbosa de Lima AG, da Silva MV, editors Numerical analysis of heat and mass transfer in porous media. Berlin: Springer-Verlag; 2012, p. 121–51.
[85] Park J, Kang MK. A numerical simulation of the resin film infusion process. Compos Struct 2003;60(4):431–7.
[86] Hirt C, Nichols B. Volume of fluid (VOF) method for the dynamics of free boundaries. J Comput Phys 1981;39(1):201–25.
[87] Wang J, Waas AM, Wang H. Experimental and numerical study on the low-velocity impact behavior of foam-core sandwich panels. Compos Struct 2013;96:298–311.
[88] Sas HS, Šimáček P, Advani SG. A methodology to reduce variability during vacuum infusion with optimized design of distribution media. Compos Part A Appl Sci Manuf 2015;78:223–33.
[89] Wang J, Simacek P, Advani SG. Use of centroidal Voronoi diagram to find optimal gate locations to minimize mold filling time in resin transfer molding. Compos Part A Appl Sci Manuf 2016;87:243–55.
[90] Lawrence JM, Fried P, Advani SG. Automated manufacturing environment to address bulk permeability variations and race tracking in resin transfer molding by redirecting flow with auxiliary gates. Compos Part A Appl Sci Manuf 2005;36(8):1128–41.
[91] Correia NC, Robitaille F, Long AC, Rudd CD, Šimáček P, Advani SG. Analysis of the vacuum infusion moulding process: I. Analytical formulation. Compos Part A Appl Sci Manuf 2005;36(12):1645–56.
[92] Yenilmez B, Senan M, Sozer ME. Variation of part thickness and compaction pressure in vacuum infusion process. Compos Sci Technol 2009;69(11–12):1710–9.
[93] Govignon Q, Bickerton S, Kelly PA. Simulation of the reinforcement compaction and resin flow during the complete resin infusion process. Compos Part A Appl Sci Manuf 2010;41(1):45–57.
[94] Nguyen QT, Vidal-Sallé E, Boisse P, Park CH, Saouab A, Bréard J, et al. Mesoscopic scale analyses of textile composite reinforcement compaction. Compos Part B Eng 2013;44(1):231–41.
[95] Ruiz E, Achim V, Soukane S, Trochu F, Bréard J. Optimization of injection flow rate to minimize micro/macro-voids formation in resin transfer molded composites. Compos Sci Technol 2006;66(3–4):475–86.
[96] Walther J. The effect of fabric and fiber tow shear on dual scale flow and fiber bundle saturation during liquid molding of textile composites [dissertation]. Newark: University of Delaware; 2011.
[97] Walther J, Simacek P, Advani SG. The effect of fabric and fiber tow shear on dual scale flow and fiber bundle saturation during liquid molding of textile composites. Int J Mater Form 2012;5(1):83–97.
[98] Pierce RS, Falzon BG, Thompson MC. A multi-physics process model for simulating the manufacture of resin-infused composite aerostructures. Compos Sci Technol 2017;149:269–79.
[99] Pierce RS, Falzon BG, Thompson MC, Boman R. Implementation of a non-orthogonal constitutive model for the finite element simulation of textile composite draping. Appl Mech Mater 2014;553:76–81.
[100] Pierce RS, Falzon BG, Thompson MC, Boman R. A low-cost digital image correlation technique for characterising the shear deformation of fabrics for draping studies. Strain 2015;51(3):180–9.
[101] Pierce RS, Falzon BG, Thompson MC. Permeability characterization of sheared carbon fiber textile preform. Polym Compos. Epub 2016 Sep 15.